

Bound states in the continuum in open acoustic resonators

A. A. Lyapina^{1,2}, D. N. Maksimov^{1,†}, A. S. Pilipchuk^{1,2} and A. F. Sadreev¹

¹L. V. Kirensky Institute of Physics, Krasnoyarsk 660036, Russia

²Siberian Federal University, Krasnoyarsk 660041, Russia

(Received 12 April 2015; revised 19 June 2015; accepted 10 August 2015;
first published online 3 September 2015)

We consider bound states in the continuum (BSCs) or embedded trapped modes in two- and three-dimensional acoustic axisymmetric duct–cavity structures. We demonstrate numerically that, under variation of the length of the cavity, multiple BSCs occur due to the Friedrich–Wintgen two-mode full destructive interference mechanism. The BSCs are detected by tracing the resonant widths to the points of the collapse of Fano resonances where one of the two resonant modes acquires infinite life-time. It is shown that the approach of the acoustic coupled mode theory cast in the truncated form of a two-mode approximation allows us to analytically predict the BSC frequencies and shape functions to a good accuracy in both two and three dimensions.

Key words: aeroacoustics, noise control, wave scattering

1. Introduction

Bound states in the continuum (BSCs), also known as embedded trapped modes, are localized solutions which correspond to discrete eigenvalues coexisting with extended modes of a continuous spectrum in resonator–waveguide configurations. The existence of trapped solutions residing in the continuum was first reported by von Neumann & Wigner (1929) at the dawn of quantum mechanics. To the best of our knowledge, the term bound state (embedded) in the continuum was introduced by Fonda (1961) in the context of resonance reactions in the presence of continuous channels. Since then the bound state in the continuum has been universally used to designate a BSC in quantum mechanics (Stillinger & Herrick 1975). In the field of fluid mechanics, Parker (1966, 1967) is credited with being the first to encounter resonances of pure acoustic nature in air flow over a cascade of flat parallel plates. Nowadays, the BSCs are known to exist in various waveguide structures ranging from quantum wires (Shahbazyan & Raikh 1994; Kim, Satanin, Joe & Cosby 1999; Olendski & Mikhailovska 2002; Sadreev, Bulgakov & Rotter 2006; Cattapan & Lotti 2007), to acoustic waveguides (Duan *et al.* 2007; Linton & McIver 2007; Hein & Koch 2008; Hein, Koch & Nannen 2012), and photonic crystals (Shipman & Venakides 2005; Bulgakov & Sadreev 2008; Marinica, Borisov & Shabanov 2008; Yang *et al.* 2014). The BSCs are of immense interest, specifically in optics thanks to

†Email address for correspondence: mdn@tnp.krasn.ru

the experimental opportunity to confine light in optical microcavities despite outgoing waves being allowed in the surrounding medium (Plotnik *et al.* 2011; Hsu *et al.* 2013; Corrielli *et al.* 2013; Weimann *et al.* 2013; Zhang & Zhang 2015). At the same time, in aerodynamics, trapped and nearly trapped modes are known to cause severe vibrations and noise problems in gas and steam pipelines (Jungowski, Botros & Studzinski 1989; Ziada & Bühlmann 1992; Kriesels *et al.* 1995; Ziada & Shine 1999; Tonon *et al.* 2011).

The most trivial mechanism of BSC formation is due to the symmetry of the structure, i.e. the BSC and the continuous-spectrum modes have incompatible symmetries. Typically, when symmetric and antisymmetric problems are separated the first symmetric and antisymmetric propagating modes have different cut-off frequencies. Thus, the difference between the cut-off frequencies provides a window for an antisymmetric BSC to reside in. Such BSCs are omnipresent in wave-related set-ups, including quantum wires (Schult, Ravenhall & Wyld 1989), fluid in a wave tank (Evans & Linton 1991), and acoustic (Evans, Levitin & Vassiliev 1994; Sugimoto & Imahori 2005) and elastic (Maksimov & Sadreev 2006) waveguides.

By breaking the axial symmetry of the structure the symmetry protected BSCs become quasi-trapped leaky modes coupled to the propagating modes of the waveguides (Aslanyan, Parnovski & Vassiliev 2000). Nöckel (1992) and Ladrón de Guevara, Claro & Orellana (2003) demonstrated that if the symmetry is broken under variation of a control parameter the symmetry protected BSCs reveal themselves in the form of ghost Fano resonances. Conversely, as the symmetry is recovered the Fano resonance collapses with one of the two resonant modes acquiring an infinite life-time. The collapse of Fano resonance is a signature of full destructive interference of two degenerate eigenmodes of the resonator on the waveguide–resonator interface (Kim *et al.* 1999). As a consequence of this a trapped mode is formed as a localized solution decoupled from the extended modes of the waveguides. Importantly, the full destructive interference of two degenerate eigenmodes leaking into waveguides represents a generic mechanism of BSC formation (Friedrich & Wintgen 1985) whose implementation goes far beyond the above symmetry arguments by Ladrón de Guevara *et al.* (2003). In particular, this mechanism allows the formation of BSCs with the same symmetry about the duct axis as the coexisting scattering solution (Hein *et al.* 2012). The BSCs which can be attributed to a full destructive interference are frequently reported in quantum mechanics (Kim *et al.* 1999), optics (Bulgakov & Sadreev 2014), and acoustics (Hein, Koch & Nannen 2010; Hein *et al.* 2012). The same interference mechanism was recently employed by Lepetit *et al.* (2010) and Lepetit & Kanté (2014) for experimental observation of BSCs in microwave set-ups. Throughout this paper the full destructive interference of two degenerate modes resulting in the formation of BSCs in multimodal cavities will be invoked to establish a two-mode approximation that will be used for finding BSC frequencies and shape functions.

In our recent work (Maksimov *et al.* 2015) we showed that the approach known in quantum mechanics as formalism of the effective non-Hermitian Hamiltonian (Dittes 2000; Pichugin, Schanz & Seba 2001) could be adapted for solving the hard-wall acoustic cavity–duct problem. The essential feature of the approach is that it allows one to recover transmission spectra of open-boundary systems relying on the spectral properties of their closed counterparts. Technically, the method is the acoustic coupled mode theory in which the pressure field within the cavity is represented by the modal variables corresponding to the amplitudes of the eigenmodes of the closed cavity decoupled from waveguides. We also refer the reader to the

paper by Racec, Racec & Neidhardt (2009) for a similar approach for scattering in cylindrical nanowire heterostructures.

In this paper, we consider the acoustical problem of axisymmetric side-branch cavities in two- and three-dimensional ducts of infinite length. Our primary goal is to explore the interference phenomena resulting in the formation of BSCs localized within two- and three-dimensional cavities. The BSCs will be analysed in the framework of the acoustic coupled mode theory (Maksimov *et al.* 2015). We will demonstrate that our approach not only represents an alternative numerical technique for finding BSCs but also provides an efficient analytical tool for construction the BSC shape function in the two-mode approximation. In particular, we will see that the two-mode approximation is able, to a good accuracy, to reproduce the BSC pressure field within two- and three-dimensional acoustic cavities.

The paper is organized as follows. In §2 we provide a brief overview of the acoustic coupled mode theory which is our major tool for analysing the scattering problem. The numerical techniques for finding BSCs are also discussed. In §3 we present our results on BSCs in two-dimensional duct–cavity systems. Three-dimensional systems are considered in §4. Finally, we conclude in §5.

2. Acoustic coupled mode theory

Let us start with the formulation of the problem. Throughout this paper we adopt non-dimensionalized quantities. After the time dependence is removed through the substitution $\psi(t) = \psi \exp(-i\omega t)$, the pressure field ψ within a cavity–duct structure is controlled by the non-dimensional stationary Helmholtz equation

$$\left(\frac{\partial^2}{\partial x^2} + \frac{\partial^2}{\partial y^2} + \frac{\partial^2}{\partial z^2} \right) \psi + \omega^2 \psi = 0, \quad (2.1)$$

where ω is the non-dimensional frequency. The x -axis is aligned with the centreline of the duct–cavity structure. The problem could be reduced to two dimensions under assumption that the structure has constant thickness along the z -axis which allows us to present the solution of (2.1) as $\psi = \psi(x, y)\psi(z)$. In what follows we take $\psi(z) = \text{const.}$ which means that only the first propagating mode is involved.

Equation (2.1) has to be solved subject to Neumann boundary conditions on all sound-hard boundaries of the cavity and reflectionless boundary conditions on the cavity–waveguide interfaces. There are numerous numerical techniques for imposing reflectionless conditions on waveguide–cavity interfaces, the most efficient of which implement layers of absorbing medium with complex refractivity giving rise to perfectly matched layers (Berenger 1994) or complex scaling (Moiseyev 1998) methods. For detailed information on the use of these methods for finding acoustic BSCs we refer the reader to the papers by Hein & Koch (2008), Hein *et al.* (2012) which thoroughly review the subject. In this paper we will use an alternative method, namely acoustic coupled mode theory (Maksimov *et al.* 2015). The method is a recent adaptation of the approach known in quantum mechanics as formalism of the effective non-Hermitian Hamiltonian. In this section we only briefly review the essentials and introduce the basic concepts that will be needed later on for understanding the mechanism of BSC formation.

To be consistent with the further applications our approach is exemplified on the two-dimensional duct–cavity structure depicted in figure 1 where we show a two-dimensional cavity of length L_x and width L_y coupled to symmetrically

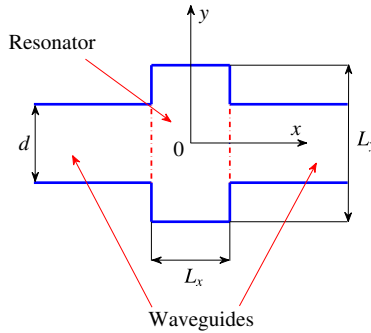


FIGURE 1. (Colour online) Structure lay-out. $d = 1$.

positioned waveguides of width d . In what follows we take $d = 1$. As mentioned in the Introduction the coupled mode theory relies on the spectral properties of a closed cavity decoupled from the waveguides. In that context closed means that in the first step the eigenmodes and eigenfrequencies of the cavity are computed with the Neumann boundary conditions

$$\frac{\partial \psi}{\partial \sigma} \Big|_{\partial \Omega} = 0 \tag{2.2}$$

on the boundary of the resonator $\partial \Omega$, including the waveguide–cavity interfaces as well as the physical boundaries; σ is the local coordinate normal the boundary of the closed resonator. In the case of a rectangular cavity the eigenvalue problem is easily solved analytically to yield the spectrum as

$$\omega_{n,m}^2 = \left(\frac{\pi(n-1)}{L_x} \right)^2 + \left(\frac{\pi(m-1)}{L_y} \right)^2, \quad n, m = 1, 2, \dots \tag{2.3}$$

At the same time the eigenmodes are found as products of two factors:

$$\psi_{n,m} = \sqrt{\frac{(2 - \delta_n^1)(2 - \delta_m^1)}{L_x L_y}} \cos \left(\frac{\pi(n-1)(2x + L_x)}{2L_x} \right) \cos \left(\frac{\pi(m-1)(2y + L_y)}{2L_y} \right), \tag{2.4}$$

where δ_n^n is the Kronecker delta. Note that the eigenfunctions are unit-normalized, so that

$$\int \psi_{n,m}^2 \, dx \, dy = 1. \tag{2.5}$$

The propagating solutions in the waveguides have the form of plane waves:

$$\phi_p^{(\pm)}(x, y) = \sqrt{\frac{1}{4\pi k_p}} \exp(\pm i k_p x) \chi_p(y), \tag{2.6}$$

where symbol $+(-)$ stands for waves propagating to the right (left), and the functions $\chi_p(y)$ are defined as

$$\chi_p(y) = \sqrt{2 - \delta_p^1} \cos \left(\pi \frac{(p-1)(2y+1)}{2} \right). \tag{2.7}$$

The dispersion relation is

$$k_p = \sqrt{\omega^2 - \pi^2(p-1)^2}, \quad p = 1, 2, \dots \quad (2.8)$$

The pressure field within the cavity ψ_c could be constructed as a modal expansion

$$\psi_c = \sum_{n,m} g_{n,m} \psi_{n,m} \quad (2.9)$$

over eigenfunctions (2.4). The key equation for finding the unknowns $g_{n,m}$ for the cavity excited by an incoming wave has the following form (Maksimov *et al.* 2015):

$$(\mathbf{D} - \omega^2 \mathbf{I}) \mathbf{g} = -i \sum_{p=1}^{\infty} \sqrt{\frac{k_p}{\pi}} \sum_{C=L,R} \mathbf{v}_{C,p} a_{C,p}, \quad (2.10)$$

where \mathbf{I} is the identity matrix, the subscript $C = L, R$ specifies the coupling with the left and right waveguides, and the unknown vector \mathbf{g} contains the coefficients $g_{n,m}$. Analogously, the amplitudes $a_{C,p}$ are the coefficients of the modal expansion of the incident wave field in the waveguides over the eigenfunctions (2.6), while the vector $\mathbf{v}_{C,p}$ contains the coupling constants $v_{C,p}^{m,n}$ between the specific eigenmode (m, n) (2.4) and the (C, p) propagating mode of the waveguides (2.6). Finally, the matrix \mathbf{D} has the following form:

$$\mathbf{D} = \boldsymbol{\Omega}^2 - \sum_p i k_p \sum_{C=L,R} \mathbf{v}_{C,p}^\dagger \mathbf{v}_{C,p}, \quad (2.11)$$

where $\boldsymbol{\Omega}^2$ is a diagonal matrix which carries the squared eigenfrequencies $\omega_{n,m}^2$ (2.3) on the main diagonal and the symbol \dagger stands for Hermitian transpose. Notice that the coupling to the evanescent modes $(p-1)\pi > \omega$ of the waveguides is accounted for in (2.11) by the terms with imaginary wavenumbers k_p found from (2.8). At this point we only have to specify the coupling constants $v_{C,p}^{m,n}$. According to Pichugin *et al.* (2001) and Maksimov *et al.* (2015) they are evaluated as overlapping integrals between the functions (2.7) and the eigenfunctions (2.4) on the waveguide–cavity interface:

$$v_{C,p}^{m,n} = \int \chi_p \psi_{m,n} d\tau_C, \quad (2.12)$$

where τ_C is the local interface coordinate orthogonal to the wave vector. The generalization to the three-dimensional case is straightforward; the coupling constant is a surface integral (Maksimov *et al.* 2015) with τ_C representing the local coordinate set on a flat waveguide-resonator interface. Notice that (2.10) formally contains an infinite number of unknowns. However, as it was demonstrated in Maksimov *et al.* (2015), for computational ease the basis can be truncated to a reasonably small number of modes in a given frequency window. After the unknown vector \mathbf{g} is obtained from (2.10) the coefficients of the modal expansion of the outgoing field in the waveguide $b_{C,p}$ are found as

$$b_{C,p} = -a_{C,p} + \sqrt{4\pi k_p} \mathbf{v}_{C,p}^\dagger \mathbf{g}. \quad (2.13)$$

The above described approach has been demonstrated to be applicable to finding scattering functions and reflection amplitudes in two- and three-dimensional cavities

(Maksimov *et al.* 2015). The goal of the present paper, however, is to adapt it for computing BSCs. The BSCs are localized solutions of infinite life-time which exist in the cavity even when no incident field is present in the waveguides. Thus, according to (2.10) one obtains an eigenvalue problem

$$(\mathbf{D} - z_n^2 \mathbf{I})g_n = 0. \quad (2.14)$$

When an eigenvalue $z_n = \omega_n + i\gamma_n$ found from (2.14) is real its eigenvector g_n corresponds to a BSC. Unfortunately, (2.14) does not represent the standard eigenvalue problem because the matrix \mathbf{D} (2.11) depends on the spectral parameters k_p which are linked to the eigenvalue z_n through the dispersion relation (2.8). One of the possible solutions (Sadreev *et al.* 2006) is to employ an iterative procedure of solving the fixed-point equation for real eigenvalues of (2.14). Alternatively, one of the most efficient techniques for finding complex eigenvalues (2.14) is the harmonic inversion method which allows one to extract the positions and life-times of the resonances from the response of the system to an external driving. In this paper we do not detail the harmonic inversion method as Wiersig & Main (2008) nicely outline it in their paper on the fractal Weyl law for chaotic microcavities. In brief, the first step in the method is solving (2.10) with some, quite arbitrary, right-hand side which, in particular, could be a point source placed within the open cavity. The response obtained is then Fourier-transformed to yield a set of nonlinear equation for eigenvalues z_n which is subsequently solved by the use of Padé approximants (Wiersig & Main 2008).

To conclude this section we return to the Friedrich–Wintgen two-mode interference mechanism of BSC formation (Friedrich & Wintgen 1985). Let us check whether it is possible that only two modes ψ_1 and ψ_2 of the closed cavity with eigenfrequencies ω_1 and ω_2 contribute to a BSC. Suppose that only the first scattering channel with the wavenumber k_1 is open at the frequency of interest. Then, under a further assumption that the coupling to the evanescent channels $p > 1$ can be neglected we rewrite (2.14) as an eigenvalue problem for matrix \mathbf{D} with real-valued terms ω_j^2 arranged along the main diagonal in ascending order:

$$\mathbf{D} = \begin{pmatrix} \ddots & \vdots & \vdots & \vdots & \vdots & \ddots \\ \dots & \omega_0^2 - ik_1 2v_0^2 & -ik_1 2v_0 v_1 & -ik_1 2v_0 v_2 & -ik_1 2v_0 v_3 & \dots \\ \dots & -ik_1 2v_0 v_1 & \omega_1^2 - ik_1 2v_1^2 & -ik_1 2v_1 v_2 & -ik_1 2v_1 v_3 & \dots \\ \dots & -ik_1 2v_0 v_2 & -ik_1 2v_1 v_2 & \omega_2^2 - ik_1 2v_2^2 & -ik_1 2v_2 v_3 & \dots \\ \dots & -ik_1 2v_0 v_3 & -ik_1 2v_1 v_3 & -ik_1 2v_2 v_3 & \omega_3^2 - ik_1 2v_3^2 & \dots \\ \ddots & \vdots & \vdots & \vdots & \vdots & \ddots \end{pmatrix}, \quad (2.15)$$

where ω_0 and ω_3 are the eigenfrequencies next to ω_1 and ω_2 , and $v_j = v_{L,1}^{m,n}$ is the coupling constant with the open propagation channel $p=1$. Notice that above we have assumed that the absolute values of the coupling constants on the left and the right are identical, i.e. all eigenmodes have compatible symmetry about the y -axis. In fact, the matrix \mathbf{D} is split into two decoupled sub-blocks corresponding to the y -symmetric and y -antisymmetric eigenmodes so that the y -symmetric and y -antisymmetric problems could be considered independently from one another. Under variation of some control parameter, say the length of the cavity L_x , one can reach the degeneracy point where

p	(n, m)							
	(1, 1)	(1, 2)	(1, 3)	(1, 4)	(4, 1)	(4, 2)	(2, 3)	(2, 4)
1	0.408	0	-0.367	0	0.577	0	-0.520	0
2	0	0.245	0	-0.441	0	0.346	0	-0.624
3	0	0	0.173	0	0	0	0.245	0
4	0	0.021	0	0.082	0	0.030	0	0.116
5	0	0	0.034	0	0	0	0.049	0
6	0	0.007	0	0.024	0	0.011	0	0.034

TABLE 1. Numerical values of coupling constants $v_{L,p}^{n,m}$ at $L_x = 3, L_y = 2$.

$\omega_1 = \omega_2 = \omega_{BSC}$; then the matrix (2.15) has a real eigenvalue ω_{BSC}^2 with the eigenvector

$$\mathbf{g} = \frac{v_1 v_2}{\sqrt{v_1^2 + v_2^2}} (\dots, 0, 1/v_1, -1/v_2, 0, \dots)^\dagger \quad (2.16)$$

containing only two non-zero entries. Thus, the corresponding BSC shape function can be constructed as

$$\psi_{BSC} = \frac{v_1 v_2}{\sqrt{v_1^2 + v_2^2}} \left(\frac{1}{v_1} \psi_1 - \frac{1}{v_2} \psi_2 \right). \quad (2.17)$$

The above equation represents the central mathematical result to be used for analyzing BSCs in open acoustic resonators. In essence, it manifests the well-known interference mechanism (Friedrich & Wintgen 1985). In fact, both eigenmodes ψ_1 and ψ_2 , albeit coupled to the waveguides, contribute to (2.17) in the proportion providing full destructive interference at the degeneracy point so that the resulting BSC function ψ_{BSC} is decoupled from the open channel. For details on the realization of the above mechanism in the field of quantum mechanics we refer the reader to the paper by Sadreev *et al.* (2006). We mention in passing that thanks to the symmetry about the duct axis the same arguments are valid for the duct-axis antisymmetric modes with k_1 replaced by k_2 according to (2.8).

The above result (2.17) is exact under the assumption that the coupling to the evanescent channels could be neglected. However, we would like to remind the reader that the evanescent eigenmodes are present in summation over index p on the right-hand side of (2.11). Therefore (2.17) is not an exact solution, and can only be seen as the basis for a two-mode approximation for BSCs occurring at the degeneracy points. Some remarks are due on the validity of the two-mode approximation. As will be seen later on, due to the structure of (2.11) the evanescent coupling results in the presence of modes other than the two basic modes in the modal expansion of the BSC shape function, as well as in a shift of the true BSC point from the degeneracy point. Nevertheless, one can argue that the coupling to the evanescent channels is small relative to the coupling to the open channel as we consider the eigenmodes residing in the frequency window where only one symmetric and one antisymmetric propagating channel are open. In order to illustrate this we collect in table 1 the numerical values of the coupling constants for some relevant eigenmodes evaluated on the basis of the analytical results from Maksimov *et al.* (2015). One can see from table 1 that the coupling constants rapidly decay with the growth of the channel number p . In fact, it can be demonstrated that any coupling constant decays away from its maximal value with the asymptotic law $v_{L,p}^{n,m} \sim 1/p^2$.

Finally, notice that the two-mode approximation has no restrictions related to the size of the cavity. One can see from (2.15) that once a degeneracy occurs in the closed cavity it always results in the formation of a BSC through the Friedrich–Wintgen mechanism irrespective of the values of L_x , and L_y . If the size of the cavity is isometrically increased while the width of the waveguide is kept unchanged, the eigenfrequencies next to the BSC eigenfrequencies ω_0 , ω_3 would shift closer to the BSC eigenfrequency. The real-valued diagonal term in (2.14) will decrease as $(\omega_{0,3}^2 - \omega_{BSC}^2) \sim 1/S$, $S = L_x L_y$ because the mean distance between the eigenfrequencies is inversely proportional to the width/length of the cavity. On the other hand the coupling constants v_j in matrix \mathbf{D} (2.15) will decrease as $v_j \sim 1/\sqrt{S}$ because the eigenfunctions (2.4) contributing to the overlapping integrals (2.12) have the normalization constant \sqrt{S} in the denominator. As a consequence of this the off-diagonal terms $v_j v_{j'}$ in matrix (2.15) decrease as $v_j v_{j'} \sim 1/S$. One can see that the coupling of the BSC eigenmodes ψ_0 , ψ_3 next to the basic BSC modes ψ_1 , ψ_2 through the evanescent channels decreases at the same rate as the resonant term $\omega_{0,3}^2 - \omega_{BSC}^2$. This leads us to the conclusion that the two-mode approximation does not break down as the size of the cavity is increased. Notice that the same holds true in the three-dimensional case where the coupling constant decreases as $v_j \sim 1/\sqrt{V}$, with V being the volume of the cavity.

3. Bound states in the continuum in two-dimensional open cavities

We start by computing the transmittance $T = |b_{1,R}|^2$ for the two-dimensional cavity in figure 1 under the assumption that an incident wave in the first propagation band $p=1$ enters the cavity from the left waveguide. For solving the scattering problem we used the approach described in §2. The numerical values of the coupling constants $v_{C,p}^{n,m}$ in (2.10), (2.11) are taken from our previous work (Maksimov *et al.* 2015). In figure 2 we demonstrate the dependence of the transmittance T on the frequency of the incoming wave ω and the length of the cavity L_x . Notice that the frequency varies in the range $[0, 2\pi]$ which means according to (2.8) that only one symmetric scattering channel is open in each waveguide. In figure 2 we also depict the frequencies of the eigenmodes of the closed cavity symmetric about the duct axis (2.3) $m = 1, 3, 5, \dots$. The eigenfrequencies which correspond to the modes symmetric about the y -axis, to be referred to below as y -symmetric, are shown by dashed lines. The solid lines show the eigenfrequencies of y -antisymmetric eigenmodes. One can see that the degeneracy points of eigenfrequencies with the same symmetry about the y -axis coincide with an abrupt change of the transmittance; the transmittance drops from unity to zero as the frequency is swept across the point where the collapse of Fano resonance occurs.

The complex resonance frequencies for the cavity are computed by the harmonic inversion method. In the given range of parameters we found five BSCs. Three of them originate from the modes symmetric about the y -axis (shown by circles) and two from the antisymmetric ones (shown by stars). For further convenience we number the BSCs from 1 to 5. The complex eigenfrequencies are plotted against the length of the resonator L_x in figure 3 where one can see that the imaginary part γ_n goes to zero as one approaches the BSC point. In figure 4 we demonstrate the numerical solution for BSC 3 along with the corresponding coefficients of the modal expansion $g_{n,m}$ (2.9). One can clearly see that only two eigenmodes dominate in the BSC function ψ_{BSC} . The y -antisymmetric BSC 3 in figure 4 is formed by eigenmodes $\psi_1 = \psi_{4,1}(x, y)$ and $\psi_2 = \psi_{2,3}(x, y)$, with the corresponding coupling constants $v_1 = v_{L,1}^{4,1} = -v_{R,1}^{4,1} = 0.600$

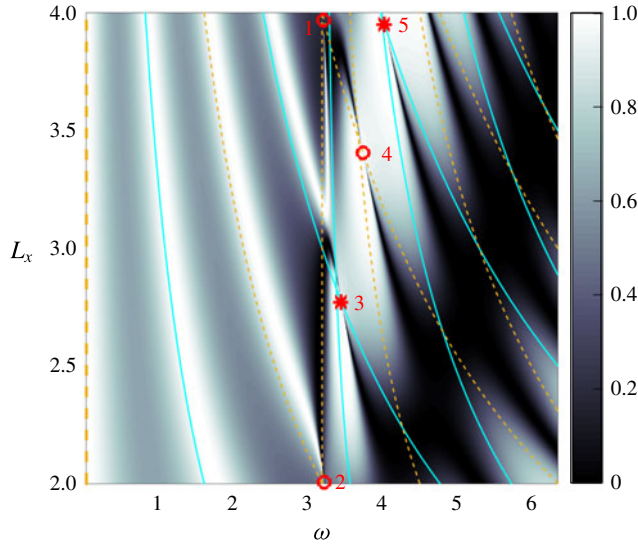


FIGURE 2. (Colour online) Transmittance for a two-dimensional cavity of length $L_y = 2$. Only the first symmetric channel with $p = 1$ is open. The dashed lines show eigenfrequencies of the modes symmetric about the y -axis; the solid lines show antisymmetric ones. The positions of the BSCs are shown by open circles and stars for y -symmetric and y -antisymmetric modes, respectively.

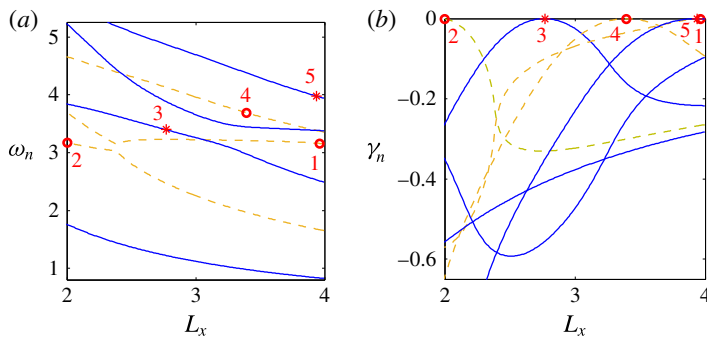


FIGURE 3. (Colour online) Complex eigenfrequencies against the length of the two-dimensional resonator L_x : (a) real part; (b) imaginary part. The y -symmetric resonances are shown by dashed lines; the y -antisymmetric ones by solid lines. The positions of BSCs from figure 2 are shown by open circles and stars for y -symmetric and y -antisymmetric modes, respectively.

and $v_2 = v_{L,1}^{2,3} = -v_{R,1}^{2,3} = -0.540$. To assess the accuracy of the two-mode approximation we introduce parameters

$$\Delta\omega = \frac{|\omega_{BSC} - \omega^*|}{\omega_{BSC}} \quad (3.1)$$

and

$$\Delta L_x = \frac{|L_x - L_x^*|}{L_x}, \quad (3.2)$$

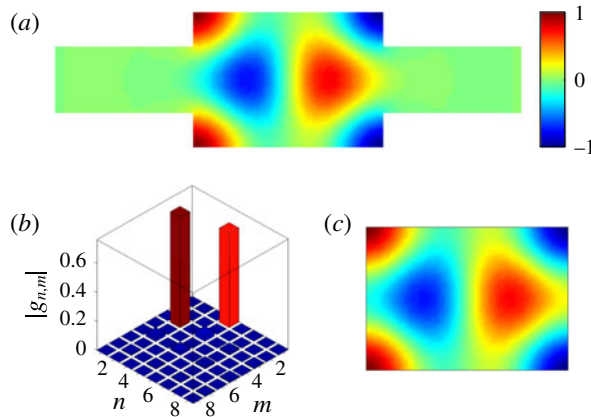


FIGURE 4. (Colour online) BSC 3, symmetric about the duct axis of a two-dimensional duct–cavity structure with $\omega_{BSC} = 3.396$, $L_y = 2$, $L_x = 2.776$: (a) pressure field of the numerically computed BSC shape function; (b) absolute values of the modal coefficients $g_{n,m}$ of the numerically computed pressure field (2.9); (c) BSC shape function found from the two-mode approximation (2.17).

with ω^* and L_x^* respectively the frequency and the length of the cavity corresponding to the degeneracy point at which the BSC would occur according the two-mode approximation (2.15). For BSC 3 we obtained $\Delta\omega = 0.019$ and $\Delta L_x = 0.018$. In figure 4 we also plot the BSC shape function constructed by (2.17). One can see from figure 4 that the two-mode approximation reproduces our numerical result to a good accuracy. We found that the same holds true for the other four BSCs in figure 2. Therefore, the other BSC functions are not presented in this paper.

The same procedure was repeated in the case of the incoming wave in the first antisymmetric channel for cavities with $L_y = 2$. As before we observed that the two-mode approximation is valid in the situation when only one antisymmetric channel is open in each waveguide. For brevity we omit a detailed description of our findings, restricting ourselves to one example of a duct-axis antisymmetric BSC, shown in figure 5. The y -symmetric BSC in figure 5 is formed by eigenmodes $\psi_1 = \psi_{5,2}(x, y)$ and $\psi_2 = \psi_{3,4}(x, y)$, with the corresponding coupling constants $v_1 = v_{L,1}^{5,2} = v_{R,1}^{5,2} = -0.692$ and $v_2 = v_{L,1}^{3,4} = v_{R,1}^{3,4} = 0.384$. For the corresponding relative errors (3.1), (3.2) we found $\Delta\omega = 0.004$ and $\Delta L_x = 0.004$. As mentioned in § 2, we expect that the two-mode approximation could be applied irrespective of the cavity size. This is confirmed by numerical tests for larger cavities $L_y = 4$. As an example, in figure 6 we present the duct-axis antisymmetric BSC formed by eigenmodes $\psi_1 = \psi_{5,8}(x, y)$ and $\psi_2 = \psi_{7,6}(x, y)$, with the coupling constants $v_1 = v_{L,1}^{5,8} = v_{R,1}^{5,8} = -0.371$ and $v_2 = v_{L,1}^{7,6} = v_{R,1}^{7,6} = 0.402$. The values of the relative errors $\Delta\omega = 0.003$ and $\Delta L_x = 0.007$ indicate that the two-mode approximation holds true for larger cavities.

As mentioned in the Introduction, the occurrence of a BSC is associated with a collapse of Fano resonance. To illustrate this, in figure 7 we plot the transmittance versus frequency for three different lengths of the resonator L_x close to the BSC points. It was recently demonstrated by Bulgakov & Sadreev (2014) that if the BSC point is approached in the parametric space along a certain path corresponding to

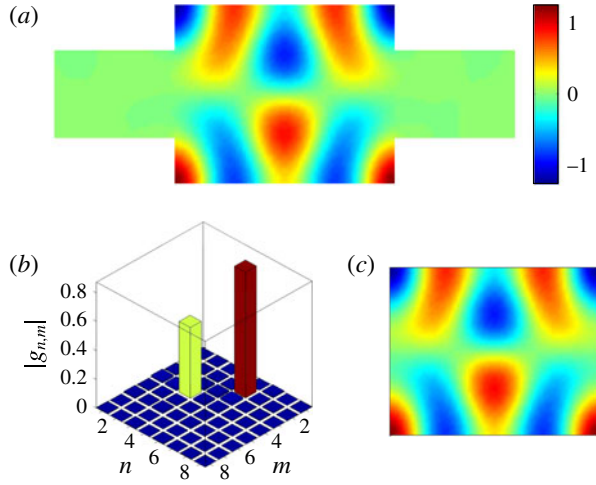


FIGURE 5. (Colour online) Bound state in the continuum antisymmetric about the duct axis of a two-dimensional duct–cavity structure with $\omega_{BSC} = 5.385$, $L_y = 2$, $L_x = 2.441$: (a) pressure field of the numerically computed BSC shape function; (b) absolute values of the modal coefficients $g_{n,m}$ of the numerically computed pressure field; (c) BSC shape function found from the two-mode approximation (2.17).

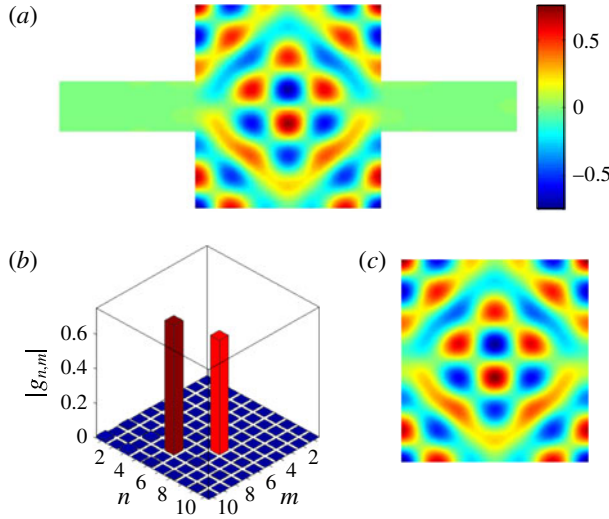


FIGURE 6. (Colour online) Bound state in the continuum antisymmetric about the duct axis of a two-dimensional duct–cavity structure with $\omega_{BSC} = 6.502$, $L_y = 4$, $L_x = 3.627$: (a) pressure field of the numerically computed BSC shape function; (b) absolute values of the modal coefficients $g_{n,m}$ of the numerically computed pressure field; (c) BSC shape function found from the two-mode approximation (2.17).

the peak of the Fano resonance, the long-lived complex mode related to the BSC provides the dominant contribution to the scattering function. In consequence the scattering function near the BSC point bears the maximal resemblance to the BSC if the parameters are tuned to the peak of the Fano resonance. This is illustrated in

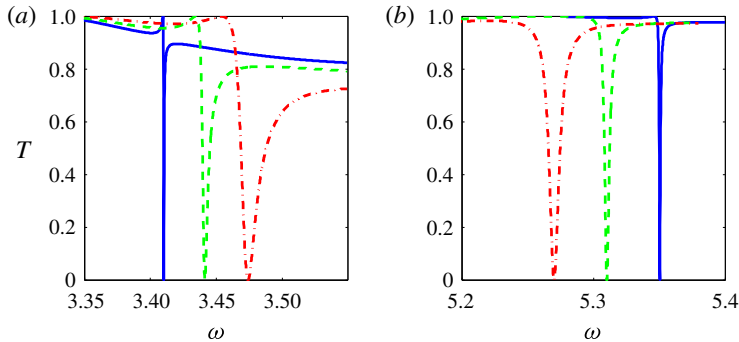


FIGURE 7. (Colour online) Collapse of Fano resonance in the vicinity of a BSC point under variation of the length of the resonator L_x . (a) BSC 4 in figure 4 with $\omega_{BSC} = 3.396$, $L_y = 2$, $L_x = 2.776$. Resonator lengths: $L_x = 2.75$, solid line; $L_x = 2.70$, dashed line; $L_x = 2.60$, dash-dot line. (b) Duct-axis antisymmetric BSC in figure 5 with $\omega_{BSC} = 3.384$, $L_y = 2$, $L_x = 2.441$. Resonator lengths: $L_x = 2.460$, solid line; $L_x = 2.485$, dashed line; $L_x = 2.510$, dash-dot line.

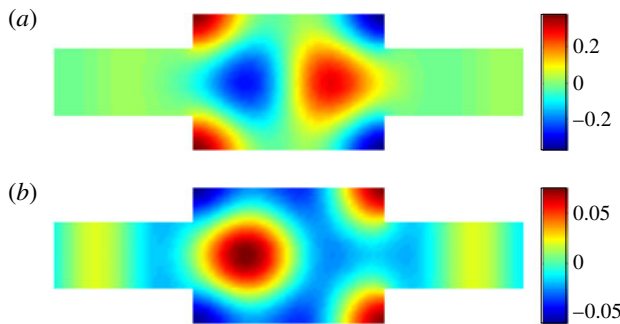


FIGURE 8. (Colour online) Scattering function at the peak $\omega = 3.410$ of the Fano resonance in figure 7 related to BSC 3 shown in figure 4. $L_y = 2$, $L_x = 2.75$. (a) Real part; (b) imaginary part.

figure 8, where one can see that the real part of the scattering function is almost identical to the BSC from figure 4, whereas the imaginary part is present as a background providing the net power flux in the system. Thus, one can experimentally observe a signature of a BSC in the form of a large-amplitude acoustic resonance even though in a realistic set-up the parameters are always detuned from the true BSC point due, for example, to fabrication inaccuracies.

4. Bound states in the continuum in three-dimensional open cavities

Let us consider the axisymmetric cylindrical resonator with two coaxially attached cylindrical waveguides of radius $a = 1$ as depicted in figure 9(a). After the azimuthal variable is separated out we can restrict ourself to the case of zero angular momentum, bearing in mind that our results can be easily generalized to the non-zero case by taking into account that, by virtue of (2.12), only the modes of the same rotational number are coupled on the waveguide–cavity interface. In our case the

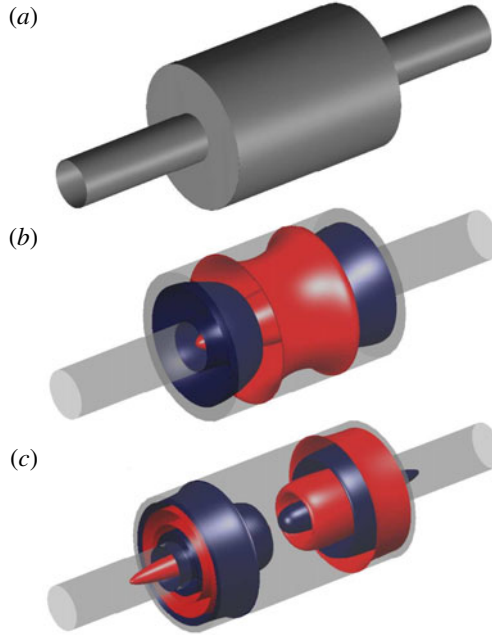


FIGURE 9. (Colour online) Bound states in the axisymmetric duct–cavity structure. (a) Cylindrical resonator of radius R and length L_x with two coaxially attached waveguides of radius $a = 1$. (b) Pressure field isosurfaces of BSC 2 in figure 12 symmetric with respect to the central section of the resonator; dark blue $\psi_{BSC} = -0.1$, light red $\psi_{BSC} = 0.1$. (c) Pressure field isosurfaces of BSC 7 in figure 13 antisymmetric with respect to the central section of the resonator; dark blue $\psi_{BSC} = -0.1$, light red $\psi_{BSC} = 0.1$.

cavity eigenfrequencies are given by

$$\omega_{m,n}^2 = \left[\frac{\mu_m^2}{R^2} + \frac{\pi^2(n-1)^2}{L_x^2} \right], \quad (4.1)$$

where R and L_x are the radius and length of the cylindrical resonator, and μ_m is the m th root of the equation $J'_0(\mu_m) = J_1(\mu_m) = 0$, $m = 1, 2, \dots$, for the derivative of the first-order Bessel function. The corresponding eigenfunctions are

$$\psi_{m,n}(r, x) = \frac{1}{\sqrt{\pi R J_0(\mu_m)}} J_0\left(\frac{\mu_m r}{R}\right) \psi_n(x), \quad (4.2)$$

where r is the radial coordinate in the y_0z -plane while the axial modes are given by

$$\psi_n(x) = \sqrt{\frac{2 - \delta_n^1}{L_x}} \cos\left(\frac{\pi(n-1)(2x + L_x)}{2L_x}\right), \quad n = 1, 2, \dots \quad (4.3)$$

As before the transmission problem was solved by the use of the acoustic coupled mode theory (Maksimov *et al.* 2015) and the complex eigenvalues were obtained by the harmonic inversion method. The frequency ω varies in the range $[0, \mu_2]$, $\mu_2 = 3.831$ which means that only one propagating channel is open in each waveguide. The transmittance, along with the spectrum of the closed resonator and the positions of

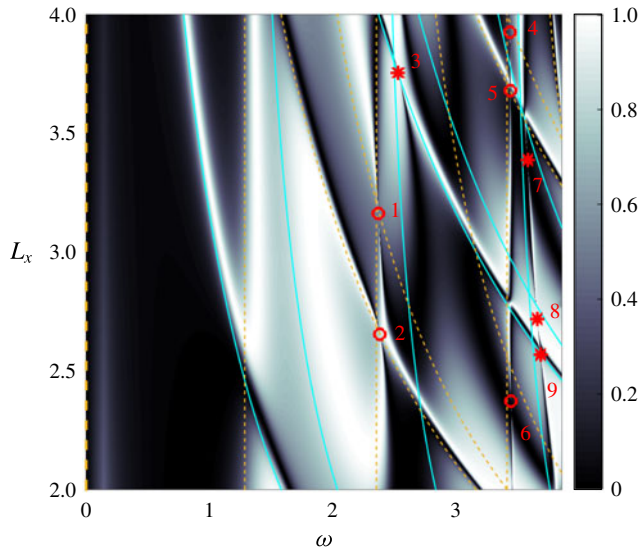


FIGURE 10. (Colour online) Transmittance for a cylindrical resonator with radius $R = 2$ with two coaxially attached cylindrical waveguides of radius $a = 1$ versus frequency ω and the length of the resonator L_x . The dashed lines show eigenfrequencies of the modes symmetric about the $y0z$ -plane; solid lines show antisymmetric ones. The positions of the BSCs are shown by open circles and stars for $y0z$ -symmetric and $y0z$ -antisymmetric modes, respectively.

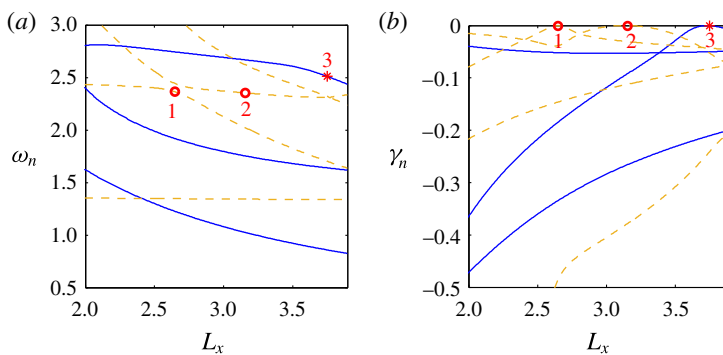


FIGURE 11. (Colour online) Complex eigenfrequencies against the length of the three-dimensional resonator L_x : (a) real part, (b) imaginary part. The $y0z$ -symmetric resonances are shown by dashed lines; $y0z$ -antisymmetric ones by solid lines. The positions of BSCs from figure 10 are shown by open circles and stars for $y0z$ -symmetric and $y0z$ -antisymmetric modes, respectively.

BSCs, is shown in figure 10. The complex eigenfrequencies are plotted in figure 11 against the length of the resonator L_x . In figures 12 and 13 we demonstrate the shape functions of two BSCs occurring through the two-mode interference mechanism. BSC 2 in figure 12 with $\Delta\omega = 0.012$ and $\Delta L_x = 0.012$ is formed by eigenmodes $\psi_1 = \psi_{1,3}(r, x)$ and $\psi_2 = \psi_{3,1}(r, x)$, with the corresponding coupling constants $v_1 = v_{L,1}^{3,1} = v_{R,1}^{3,1} = 0.310$ and $v_2 = v_{L,1}^{1,3} = v_{R,1}^{1,3} = 0.289$, while the $y0z$ -antisymmetric

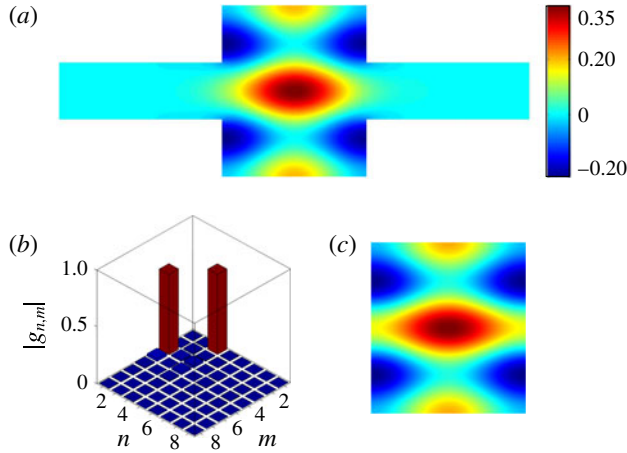


FIGURE 12. (Colour online) BSC 2 in a three-dimensional duct-cavity structure with $\omega_{BSC} = 2.367$, $R = 2$, $L_x = 2.655$: (a) $x0y$ -plane section of the pressure field of the numerically computed BSC shape function; (b) absolute values of the modal coefficients of the numerically computed pressure field; (c) BSC shape function found from the two-mode approximation (2.17).

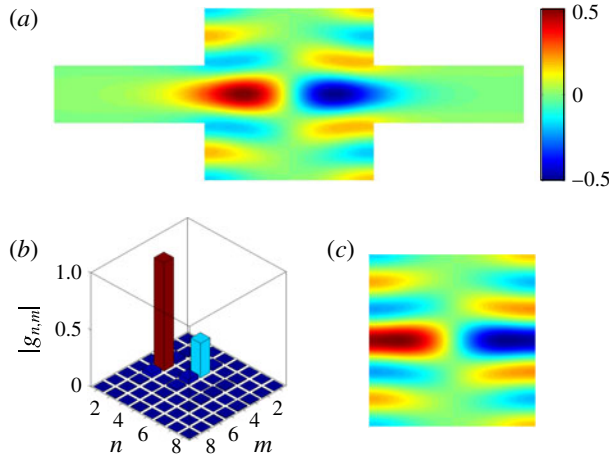


FIGURE 13. (Colour online) BSC 7 in a three-dimensional duct-cavity structure with $\omega_{BSC} = 3.557$, $R = 2$, $L_x = 3.387$: (a) $x0y$ -plane section of the pressure field of the numerically computed BSC shape function; (b) absolute values of the modal coefficients of the numerically computed pressure field; (c) BSC shape function found from the two-mode approximation (2.17).

BSC 7 depicted in figure 13 is formed by $\psi_1 = \psi_{2,4}(r, x)$ and $\psi_2 = \psi_{4,3}(r, x)$, with the coupling constants $v_1 = v_{L,1}^{2,4} = -v_{R,1}^{2,4} = -0.078$ and $v_2 = v_{L,1}^{4,3} = -v_{R,1}^{4,3} = 0.389$. A three-dimensional visualization of BSCs from figures 12 and 13 is offered in figure 9(b,c) in the form of pressure field isosurfaces. One can see that, of all the BSCs in figure 10, BSC 7 deviates the most from the corresponding degeneracy point $\Delta\omega = 0.016$ and $\Delta L_x = 0.066$. The reason for this can be understood from

figures 9(c) and 13 where one can clearly see that BSC 7 extends far into the waveguides due to the coupling to the evanescent modes which is neglected by the two-mode approximation. One can conclude that the coupling to the evanescent modes becomes important just below the next channel propagation threshold as the channel function extends far into the waveguide. Nevertheless, the two-mode approximation is still valid in the three-dimensional case, reproducing the numerically computed shape functions to a good accuracy.

In this paper, we restricted ourselves to coaxial systems in which the azimuthal number is a constant of motion so that the rotational vibration modes do not participate in the formation of BSC depicted in figures 12 and 13. It is worth noticing, however, that the cavity eigenmodes with azimuthal number $\nu \neq 0$ are symmetry-protected BSCs as their eigenfrequencies are below the ν th propagating threshold in cylindrical waveguides.

5. Conclusion

We have considered sound transmission through two- and three-dimensional acoustic resonators and demonstrated the existence of singular points at which the unit transmittance coalesces with the zero transmittance at the points of collapse of Fano resonances. These singular points occur due to a full destructive interference of two degenerate modes of the same symmetry. As a result a certain superposition of these two modes is a trapped solution corresponding to a bound state in the continuum or embedded trapped mode localized within the resonator. The above mechanism of wave localization was first proposed by Friedrich & Wintgen (1985), and so far has been experimentally realized only in microwave set-ups (Lepetit *et al.* 2010; Lepetit & Kanté 2014). In the present paper we have invited the reader to consider acoustic cylindrical resonators coaxially connected to semi-infinite waveguides where the degeneracy points could be accessed in the parametric space under variation of the length of the resonator. We speculate that such a tuning could be performed in a realistic acoustic experiment by the use of piston-like hollow-stem waveguides tightly fitted to the interior boundaries of a cylindrical cavity. For analysing the bound states in the continuum we successfully employed the acoustic coupled mode theory (Maksimov *et al.* 2015) which allowed us to analytically predict the eigenfrequencies of the bound states as well as their shape functions. Until recently (Hein *et al.* 2012) the bound states in the continuum were independently studied in physics and fluid mechanics with little or no cross-fertilization. In the present paper we have attempted to bridge that gap, to the mutual benefit of both communities.

Acknowledgement

This work has been supported by Russian Science Foundation through grant 14-12-00266.

REFERENCES

- ASLANYAN, A., PARNOVSKI, L. & VASSILIEV, D. 2000 Complex resonances in acoustic waveguides. *Q. J. Mech. Appl. Maths* **53** (3), 429–447.
- BERENGER, J.-P. 1994 A perfectly matched layer for the absorption of electromagnetic waves. *J. Comput. Phys.* **144**, 185–200.
- BULGAKOV, E. & SADREEV, A. 2008 Bound states in the continuum in photonic waveguides inspired by defects. *Phys. Rev. B* **78** (7), 075105.

- BULGAKOV, E. N. & SADREEV, A. F. 2014 Robust bound state in the continuum in a nonlinear microcavity embedded in a photonic crystal waveguide. *Opt. Lett.* **39** (17), 5212–5215.
- CATTAPAN, G. & LOTTI, P. 2007 Fano resonances in stubbed quantum waveguides with impurities. *Eur. Phys. J. B* **60** (1), 51–60.
- CORRIELLI, G., DELLA VALLE, G., CRESPI, A., OSELLAME, R. & LONGHI, S. 2013 Observation of surface states with algebraic localization. *Phys. Rev. Lett.* **111** (22), 220403.
- DITTES, F. 2000 The decay of quantum systems with a small number of open channels. *Phys. Rep.* **339** (4), 215–316.
- DUAN, Y., KOCH, W., LINTON, C. M. & MCIVER, M. 2007 Complex resonances and trapped modes in ducted domains. *J. Fluid Mech.* **571**, 119–147.
- EVANS, D. V., LEVITIN, M. & VASSILIEV, D. 1994 Existence theorems for trapped modes. *J. Fluid Mech.* **261** (1), 21–31.
- EVANS, D. V. & LINTON, C. M. 1991 Trapped modes in open channels. *J. Fluid Mech.* **225** (1), 153–175.
- FONDA, L. 1961 Resonance reactions and continuous channels. *Ann. Phys.* **12** (3), 476–484.
- FRIEDRICH, H. & WINTGEN, D. 1985 Interfering resonances and bound states in the continuum. *Phys. Rev. A* **32** (6), 3231–3242.
- HEIN, S. & KOCH, W. 2008 Acoustic resonances and trapped modes in pipes and tunnels. *J. Fluid Mech.* **605**, 401–428.
- HEIN, S., KOCH, W. & NANNEN, L. 2010 Fano resonances in acoustics. *J. Fluid Mech.* **664**, 238–264.
- HEIN, S., KOCH, W. & NANNEN, L. 2012 Trapped modes and fano resonances in two-dimensional acoustical duct-cavity systems. *J. Fluid Mech.* **692**, 257–287.
- HSU, C. W., ZHEN, B., CHUA, S.-L., JOHNSON, S. G., JOANNOPOULOS, J. D. & SOLJAČIĆ, M. 2013 Bloch surface eigenstates within the radiation continuum. *Light Sci. Appl.* **2** (7), e84.
- JUNGOWSKI, W. M., BOTROS, K. K. & STUDZINSKI, W. 1989 Cylindrical side-branch as tone generator. *J. Sound Vib.* **131** (2), 265–285.
- KIM, C., SATANIN, A., JOE, Y. & COSBY, R. 1999 Resonant tunneling in a quantum waveguide: effect of a finite-size attractive impurity. *Phys. Rev. B* **60** (15), 10962–10970.
- KRIESELS, P. C., PETERS, M. C. A. M., HIRSCHBERG, A., WIJNANDS, A. P. J., IAFRATI, A., RICCARDI, G., PIVA, R. & BRUGGEMAN, J. C. 1995 High amplitude vortex-induced pulsations in a gas transport system. *J. Sound Vib.* **184** (2), 343–368.
- LADRÓN DE GUEVARA, M., CLARO, F. & ORELLANA, P. 2003 Ghost fano resonance in a double quantum dot molecule attached to leads. *Phys. Rev. B* **67** (19), 195335.
- LEPETIT, T., AKMANOY, E., GANNE, J.-P. & LOURTIOZ, J.-M. 2010 Resonance continuum coupling in high-permittivity dielectric metamaterials. *Phys. Rev. B* **82** (19), 195307.
- LEPETIT, T. & KANTÉ, B. 2014 Controlling multipolar radiation with symmetries for electromagnetic bound states in the continuum. *Phys. Rev. B* **90** (24), 241103(R).
- LINTON, C. M. & MCIVER, P. 2007 Embedded trapped modes in water waves and acoustics. *Wave Motion* **45** (1–2), 16–29.
- MAKSIMOV, D. N. & SADREEV, A. F. 2006 Bound states in elastic waveguides. *Phys. Rev. E* **74** (1), 016201.
- MAKSIMOV, D. N., SADREEV, A. F., LYAPINA, A. A. & PILIPCHUK, A. S. 2015 Coupled mode theory for acoustic resonators. *Wave Motion* **56**, 52–66.
- MARINICA, D., BORISOV, A. & SHABANOV, S. 2008 Bound states in the continuum in photonics. *Phys. Rev. Lett.* **100** (18), 183902.
- MOISEYEV, N. 1998 Quantum theory of resonances: calculating energies, widths and cross-sections by complex scaling. *Phys. Rep.* **302**, 212–293.
- VON NEUMANN, J. & WIGNER, E. P. 1929 Über merkwürdige diskrete eigenwerte. *Z. Physik* **50**, 291–293.
- NÖCKEL, J. U. 1992 Resonances in quantum-dot transport. *Phys. Rev. B* **46** (23), 15348–15356.
- OLENSKI, O. & MIKHAILOVSKA, L. 2002 Bound-state evolution in curved waveguides and quantum wires. *Phys. Rev. B* **66** (3), 035331.
- PARKER, R. 1966 Resonance effects in wake shedding from parallel plates: some experimental observations. *J. Sound Vib.* **4** (1), 62–72.

- PARKER, R. 1967 Resonance effects in wake shedding from parallel plates: calculation of resonant frequencies. *J. Sound Vib.* **5** (2), 330–343.
- PICHUGIN, K., SCHANZ, H. & SEBA, P. 2001 Effective coupling for open billiards. *Phys. Rev. E* **64** (5), 056227.
- PLOTNIK, Y., PELEG, O., DREISOW, F., HEINRICH, M., NOLTE, S., SZAMEIT, A. & SEGEV, M. 2011 Experimental observation of optical bound states in the continuum. *Phys. Rev. Lett.* **107** (18), 183901.
- RACEC, P. N., RACEC, E. R. & NEIDHARDT, H. 2009 Evanescent channels and scattering in cylindrical nanowire heterostructures. *Phys. Rev. B* **79** (15), 155305.
- SADREEV, A., BULGAKOV, E. & ROTTER, I. 2006 Bound states in the continuum in open quantum billiards with a variable shape. *Phys. Rev. B* **73** (23), 235342.
- SCHULT, R., RAVENHALL, D. & WYLD, H. 1989 Quantum bound states in a classically unbound system of crossed wires. *Phys. Rev. B* **39** (8), 5476–5479.
- SHAHBAZIAN, T. & RAIKH, M. 1994 Two-channel resonant tunneling. *Phys. Rev. B* **49** (24), 17123–17129.
- SHIPMAN, S. & VENAKIDES, S. 2005 Resonant transmission near nonrobust periodic slab modes. *Phys. Rev. E* **71** (2), 026611.
- STILLINGER, F. & HERRICK, D. 1975 Bound states in the continuum. *Phys. Rev. A* **11** (2), 446–454.
- SUGIMOTO, N. & IMAHORI, H. 2005 Localized mode of sound in a waveguide with helmholtz resonators. *J. Fluid Mech.* **546** (1), 89–111.
- TONON, D., HIRSCHBERG, A., GOLLIARD, J. & ZIADA, S. 2011 Aeroacoustics of pipe systems with closed branches. *Noise Notes* **10** (3), 27–88.
- WEIMANN, S., XU, Y., KEIL, R., MIROSHNICHENKO, A., TÜNNERMANN, A., NOLTE, S., SUKHORUKOV, A., SZAMEIT, A. & KIVSHAR, Y. 2013 Compact surface fano states embedded in the continuum of waveguide arrays. *Phys. Rev. Lett.* **111** (24), 240403.
- WIERSIG, J. & MAIN, J. 2008 Fractal weyl law for chaotic microcavities: Fresnel's laws imply multifractal scattering. *Phys. Rev. E* **77** (3), 036205.
- YANG, Y., PENG, C., LIANG, Y., LI, Z. & NODA, S. 2014 Analytical perspective for bound states in the continuum in photonic crystal slabs. *Phys. Rev. Lett.* **113** (3), 037401.
- ZHANG, M. & ZHANG, X. 2015 Ultrasensitive optical absorption in graphene based on bound states in the continuum. *Sci. Rep.* **5**, 8266.
- ZIADA, S. & BÜHLMANN, E. T. 1992 Self-excited resonances of two side-branches in close proximity. *J. Fluids Struct.* **6** (5), 583–601.
- ZIADA, S. & SHINE, S. 1999 Strouhal numbers of flow-excited acoustic resonance of closed side branches. *J. Fluids Struct.* **13** (1), 127–142.